Loss of cohesin complex components STAG2 or STAG3 confers resistance to BRAF inhibition in melanoma

Che-Hung Shen[1], **Sun Hye Kim**[1], **Sebastian Trousil**[1], **Dennie T. Frederick**[2], **Adriano Piris**[3], **Ping Yuan**[1], **Li Cai**[1], **Lei Gu**[4], **Man Li**[1], **Jung Hyun Lee**[1], **Devarati Mitra**[1], **David E. Fisher**[1,2], **Ryan J. Sullivan**[2], **Keith T. Flaherty**[2], and **Bin Zheng**[1,*]

[1]Cutaneous Biology Research Center, Massachusetts General Hospital and Harvard Medical School, Charlestown, MA

[2]Department of Medical Oncology, Massachusetts General Hospital Cancer Center, Boston, MA

[3]Department of Dermatology, Brigham & Women's Hospital and Harvard Medical School, Boston, MA

[4]Division of Newborn Medicine, Boston Children's Hospital, Harvard Medical School, Boston, MA.

Abstract

The protein kinase V-Raf murine sarcoma viral oncogene homolog B (BRAF) is an oncogenic driver and therapeutic target in melanoma. Inhibitors of BRAF (BRAFi) have shown high response rates and extended survival in melanoma patients bearing tumors that express BRAF Val600 mutations, but a vast majority of these patients develop drug resistance. Here we show that loss of Stromal antigen 2 or 3 (STAG2 or STAG3), which encode subunits of the cohesin complex, in melanoma cells results in resistance to BRAFi. We identified loss-of-function mutations in STAG2 as well as decreased expression of STAG2 or STAG3 proteins in several tumor samples from patients with acquired resistance to BRAFi and in BRAFi-resistant melanoma cell lines. Knockdown of STAG2 or STAG3 decreased sensitivity of Val600Glu BRAF-mutant melanoma cells and xenograft tumors to BRAFi. Loss of STAG2 inhibited CCCTC-binding factor (CTCF)-mediated expression of dual specificity phosphatase 6 (DUSP6), leading to reactivation of ERK signaling. Our studies unveil a previously unknown genetic mechanism of BRAFi resistance and provide new insights into the tumor suppressor function of STAG2 and STAG3.

Inhibitors of the protein kinase BRAF have shown high response rates in melanoma patients bearing tumors that express BRAF Val600 mutations, but a vast majority of these patients develop drug resistance[1,2]. Several genetic mechanisms mediating resistance to BRAF inhibitors (BRAFi) have been described, including mutations in components of the MAPK pathway (NRAS, MAP2K1/2 and NF1) and the PI3K-Akt pathway (PIK3CA, PIK3R1, PTEN and Akt)[3-8]. However, a portion (18-26%) of BRAFi-resistant melanomas are not driven by any of these known resistance mechanisms[4,5,9]. Here we show that loss of Stromal antigen 2 or 3 (STAG2 or STAG3), which encode subunits of the cohesin complex[10,11], in melanoma cells results in resistance to BRAFi. We identified loss-of-function mutations in STAG2 as well as decreased expression of STAG2 or STAG3 proteins in several tumor samples from patients with acquired resistance to BRAFi and in BRAFi-resistant melanoma cell lines. Knockdown of STAG2 or STAG3 decreased sensitivity of Val600Glu BRAF-mutant melanoma cells and xenograft tumors to BRAFi. Loss of STAG2 inhibited CCCTC-binding factor (CTCF)-mediated expression of dual specificity phosphatase 6 (DUSP6), leading to reactivation of ERK signaling. Our studies unveil a previously unknown genetic mechanism of BRAFi resistance and provide new insights into the tumor suppressor function of STAG2 and STAG3[10].

To identify additional mechanisms of acquired resistance to BRAF inhibition, we performed whole exome sequencing on a pair of pre-treatment and post-relapse melanoma tumor samples from a patient treated with BRAFi vemurafenib who had a time to disease progression of 5 months. We compared the list of mutations identified exclusively in the post-relapse sample from this patient with a set of 127 significantly mutated genes (SMG) previously identified from The Cancer Genome Atlas (TCGA) Pan-cancer analysis[12] and found that there was only one SMG (*STAG2*) mutated in the post-relapse sample (Supplementary Table 1). This mutation in the *STAG2* gene (c.577G>A, p. Asp193Asn) was subsequently confirmed by Sanger sequencing. While the pre-treatment sample contains trace amount of the mutant allele, it is greatly enriched in the post-relapse sample (Fig. 1a). *STAG2* (also known as *SA2*) encodes a core subunit in the cohesin complex that regulates cohesion and segregation of sister chromatids[10,11]. Mutations in *STAG3* and other cohesin complex subunits such as *SMC1A*, *SMC3* and *RAD21* have been shown to occur frequently in various cancers, such as urothelial bladder carcinomas, Ewing sarcoma, acute myeloid leukemia, myelodysplastic syndrome and acute megakaryoblastic leukemia[13-23]. We found that the STAG2 Asp193Asn mutation decreases the binding affinity of the protein to Rad21 and SMC1A, suggesting Asp193Asn is a loss-of-function mutation (Supplementary Fig. 1a). STAG2 has two other paralogs in mammals, STAG1 and STAG3. Data from the melanoma TCGA project[24] indicated that mutation frequencies of these three genes are ~ 4%, 3% and 5%, respectively, for a total non-redundant mutation rate of ~ 10%. We therefore examined expression of all three STAG proteins in a panel of melanoma cell lines that acquired resistance to BRAFi after chronic exposure to BRAFi[25,26] and found that both STAG2 and STAG3, but not STAG1, protein levels were reduced in several BRAFi-resistant (BR) cell lines and BRAFi and MEKi-double resistant (BMR) lines compared to their drug-sensitive counterparts (Fig. 1b). We subsequently performed Sanger sequencing of all coding exons of *STAG2* and *STAG3* genes in these cell line pairs and identified a *STAG2* nonsense mutation (c.3247A>T, p.Lys1083*) in WM902-BR cells, which was not present in the parental

WM902 cells (Supplementary Fig. 1c). No mutations in *STAG3* were identified in our cell line panel. However, when we analyzed data from a published whole-exome sequencing study of 45 patients with BRAF Val600-mutant metastatic melanoma who received vemurafenib or dabrafenib monotherapy[4], we found three *STAG3* mutations in pre-treatment samples from 14 patients who developed early resistance to therapy (<12 weeks; Supplementary Table 2). We detected *STAG3* mutations in post-relapse but not pre-treatment samples from an additional 6 patients from this study (Supplementary Table 2). Although the significance of *STAG3* mutations was not reported in the original study[4], we found that two of these mutations reduced the binding affinity to Rad21 (Supplementary Fig. 1d). Lastly, we compared the expression of STAG2 and STAG3 proteins in pairs of pre-treatment and post-relapse tumor samples from patients treated with BRAFi monotherapy or BRAFi and MEKi combination therapy by immunohistochemical analysis. Four and three post-relapse samples, respectively, out of a total of 9 pairs of samples, showed decreased levels of STAG2 and STAG3 proteins, compared to their paired pre-treatment samples (Fig. 1c, Supplementary Fig. 1e). Two of these samples showed reductions in both STAG2 and STAG3 expression. We did not detect mutations in coding exons in the *STAG2* or *STAG3* genes in these post-relapse samples, suggesting their down-regulation was mediated through epigenetic mechanisms. Taken together, these results suggest that mutations in *STAG2* and *STAG3* decreased expressions of these proteins are involved in clinical development of BRAFi resistance in melanoma patients.

To examine whether loss of STAG2 or STAG3 is sufficient to confer resistance to BRAF inhibition, we used at least two independent shRNAs to knock down the expression of either STAG2 or STAG3 in various BRAF mutant melanoma cell lines and examined whether this altered their sensitivities to pharmacological inhibition of BRAF. A375 cells expressing STAG2 shRNA showed lower sensitivity to BRAFi dabrafenib compared to scrambled control shRNA in MTS-based cell viability assays (Fig. 2a). Knockdown of STAG2 also resulted in increases of basal pERK levels and reduction of the ability of dabrafenib to inhibit ERK phosphorylation in these cells (Fig. 2b). However, phospho-Akt and phospho-S6 levels were not affected by knockdown of STAG2 (Fig. 2b). Similarly, inducible expression of an independent shRNA against STAG2 also decreased the sensitivity to either dabrafenib or vemurafenib BRAFi in SKMEL28, A375 and M14 cells (Fig. 2c,d, Supplementary Fig. 2a–h). Knockdown of STAG2 also decreased the sensitivities to MEKi trametinib alone and in combination with dabrafenib in A375 cells (Supplementary Fig. 2i–l). In addition to BRAF mutant melanoma cells, we found that in NRAS mutant SKMEL30, SKMEL103 and 501MEL melanoma cells, depletion of STAG2 by shRNA also induced resistance to trametinib, as indicated by its inability to inhibit ERK phosphorylation and reduce cell viabilities in these cells (Fig. 2e,f, Supplementary Fig. 3a–e). Similar to STAG2, knockdown of STAG3 in BRAF mutant melanoma cells also resulted in decreased sensitivities to dabrafenib or vemurafenib with regard to cell viability and ERK inhibition (Fig. 2g,h and Supplementary Fig. 4a–d). Co-depletion of both STAG2 and STAG3 further reduced the ability of vermurafenib to inhibit pERK signaling in A375 cells, compared to knockdown of STAG2 or STAG3 alone (Supplementary Fig. 4e). Furthermore, we found that either STAG2 or STAG3 knockdown in A375 cells significantly impaired the changes in cell cycle progression and reduced the percentages of annexin V-positive apoptotic cells in

response to vemurafenib treatment (Supplementary Fig. 5). These data suggest that loss of STAG2 or STAG3 decreases sensitivities to BRAF pathway inhibition through reactivation of ERK signaling.

Next, we examine the effects of STAG2 and STAG3 ectopic expression on BRAFi sensitivity in BRAF mutant melanoma cells. Expression of FLAG-tagged wild-type STAG2 and STAG3, but not Lys1083* or Asp193Asn STAG2 mutants in WM902-BR cells increased the ability of vemurafenib to inhibit ERK activities and to reduce colony formation in soft agar assays (Fig. 2k,l, Supplementary Fig. 6a,b). Similar effects of ectopic expression of STAG2 or STAG3 on vemurafenib-induced ERK inhibition were also observed in HEK293 cells co-expressing BRAF Val600Glu, and in WM983-BR, M14 and LOX-IVMI cells (Supplementary Fig. 6c–g). These results further support that STAG2 and STAG3 regulate sensitivities to BRAFi in melanoma cells.

We then sought to determine whether STAG2 and STAG3 regulate responses to BRAF inhibition in melanoma *in vivo*. A375 cells inducibly expressing STAG2 shRNA were grown as xenograft tumors in nude mice to assess their sensitivities to vemurafenib. As shown in Fig. 3a, silencing of STAG2 did not significantly impact A375 xenograft tumor growth in nude mice. However, tumors with STAG2 knockdown showed significantly decreased sensitivities to vemurafenib-induced tumor shrinkage compared to controls (Fig. 3a,b). Immunohistochemical analysis revealed that pERK levels in STAG2 knockdown tumors treated with vemurafenib were higher than those in the control group (Fig. 3c). Similar effects on the responses of A375 xenograft tumors to vemurafenib were found for knockdown of STAG3 (Fig. 3d–f). Together these data support that loss of STAG2 or STAG3 decreases sensitivities of melanoma tumors to BRAF inhibition *in vivo*.

We next investigated the molecular mechanism underlying the regulation of RAF-MEKERK signaling by STAG2. We first examined the effect of STAG2 knockdown on RAS activation in melanoma cells. Knockdown of STAG2 did not affect the levels of GTP-bound RAS in A375 or SKMEL28 cells, as demonstrated in GST-RAF1-RBD (RAF1 RAS-binding domain) pull-down assays (Supplementary Fig. 7a). Because silencing of STAG2 caused significant increases of basal pERK levels (Fig. 2), we next assessed whether STAG2 regulates ERK activities through ERK phosphatases, such as DUSP4 and DUSP6, which are key players in the BRAF-MEK-ERK pathway[6]. shRNA knockdown of STAG2 or STAG3 led to significant decreases of *DUSP6* but not *DUSP4* mRNA levels in A375 and M14 melanoma cells (Fig. 4a, Supplementary Fig. 8a,b). Similar effects on DUSP6 protein levels were observed in melanoma cells with STAG2 or STAG3 knockdown (Fig. 4b,c, Supplementary Fig. 8c). In addition, we assessed the effect of STAG2 ectopic expression on DUSP6 protein abundance. Expression of wild-type STAG2, but not Lys1083* or Asp193Asn mutants increased DUSP6 protein expression in HEK293 cells (Fig. 4d). DUSP6 protein expression was also reduced in BRAFi-resistant melanoma cell lines compared to their parental BRAFi-sensitive counterparts (Supplementary Fig. 8d). These findings support the concept that STAG2 controls the expression of DUSP6 in melanoma cells.

The cohesin complex, of which STAG2 is a major component, can interact with CCCTC-binding factor (CTCF) and participate in DNA-looping interactions between promoters and distal regulatory DNA elements, hence controlling gene expression[11,27,28]. The promoter region of *DUSP6* contains a CTCF binding site (Fig. 4e) as identified in previous whole-genome ChIP-seq analyses of CTCF-binding sites[29]. We carried out ChIP analyses in A375 and M14 melanoma cells with CTCF-specific antibody and confirmed that CTCF binds to the *DUSP6* locus in these cells (Fig. 4f, Supplementary Fig. 9a). shRNA knockdown of STAG2 significantly reduced the binding of CTCF to the *DUSP6* locus, but not to the well-established CTCF binding site in the *H19* locus (Fig. 4f, Supplementary Fig. 9a). Expression of Lys1083* or Asp193Asn STAG2 mutants abolished the binding of CTCF to the *DUSP6* locus in LOX-IVMI cells, compared to cells expressing FLAG-tagged wild-type STAG2 (Fig. 4g). Likewise, we found that binding of CTCF to the *DUSP6* locus is much stronger in WM902 cells than in WM902-BR cells that carry the STAG2 Lys1083* mutation (Supplementary Fig. 9b). Finally, to determine whether DUSP6 mediates the effect of STAG2 on the BRAFi response, we over-expressed Myc-tagged DUSP6 with STAG2 shRNA in A375 cells; restoration of DUSP6 expression attenuated the induction of basal pERK level by STAG2 silencing and enhanced the ability of vemurafenib to inhibit ERK activities and to reduce clonogenic growth in cells with STAG2 knockdown (Fig. 4h,i). Similar effects of DUSP6 ectopic expression were also observed in M14, WM902-BR and WM983-BR melanoma cells (Supplementary Fig. 10a–d). However, over-expression of DUSP4 did not obviously affect ERK activities in A375 cells expressing STAG2 shRNA or scrambled control (Supplementary Fig. 10e). Taken together, our results strongly suggest that loss of STAG2 inhibits CTCF-mediated expression of DUSP6, leading to reactivation of MEK-ERK signaling in BRAFi-treated melanoma cells.

Our findings not only reinforce the concept that reactivation of ERK signaling represents a major resistance mechanism of BRAF pathway inhibition[3,6,9], but also reveal a heretofore unappreciated connection between STAG proteins and ERK signaling. With the recent advances in the field of cancer genomics, S*TAG2* and other components of the cohesin complex have emerged as frequent targets of somatic alterations in a wide variety of cancers of different origins[10,11]. In addition to a canonical function in sister chromatid cohesion and segregation, the cohesin complex plays an important role in chromatin organization and transcription[10,11]. While SMC1, SMC3 and Rad21 form the cohesin ring structure that entraps sister chromatids, STAG2 interacts with Rad21 at the base of the ring and plays a regulatory, rather than structural, role in the cohesin complex. How STAG2 exerts its tumor suppressor functions remains an open question. Sister chromatid cohesion, instead of regulation of the global transcription program, was proposed as the major tumor suppressor function of STAG2[13]. Inactivation of STAG2 caused cohesion defects and aneuploidy in glioblastoma and colorectal carcinoma cell lines[13]. However, cytogenetic abnormalities do not appear to be associated with *STAG2* mutations in leukemia, bladder cancer and Ewing sarcoma in several recent cancer genomics studies[14,18,19], suggesting that aneuploidy may not underlie the tumor suppression role of STAG2 in these cancers. Notably, CTCF- and cohesin-binding sites have been recently reported to be frequently mutated in various types of cancers[30]. Our discovery of the regulation of the ERK signaling pathway by STAG2 or STAG3 in this study not only supports a critical role of STAG2 in regulating *DUSP6* gene

expression through CTCF (Supplementary Fig. 11), but also reveals a new dimension of their tumor suppressive capacity.

Methods

Patient samples and IHC

Patients with metastatic melanoma carrying BRAFVal600 mutation (confirmed by genotyping) were enrolled on clinical trials for treatment with a BRAF inhibitor or combined BRAF and MEK inhibitors and were consented for tissue acquisition per Institutional Review Board (IRB)-approved protocol. This protocol was reviewed and approved by the Dana-Farber Cancer Institute IRB, in accordance with the applicable federal regulations set forth at 45 CFR Part 46, and 21 CFR Parts 50 and 56. All relevant clinical trials are registered at ClinicalTrials.gov. ClinicalTrials.gov numbers are as follows: NCT01006980, NCT01107418, NCT01264380, NCT01248936, NCT00949702, and NCT01072175. Tumor biopsies were performed pre-treatment and at time of progression. Formalin-fixed tissue was analyzed to confirm that viable tumor was present via hematoxylin and eosin (H&E) staining. No statistical method was used to predetermine sample size for the IHC analysis. No samples were excluded in the IHC analysis. The investigators were blinded to group allocation and outcome assessment.

Tumor biopsies were sectioned at 4 microns and stained manually with primary antibodies for STAG2 (1:100, Santa Cruz, SC-81852) and STAG3 (1:200, Abcam Ab185109) followed by a secondary horseradish peroxidase conjugated antibody (DAKO K4003- STAG3 or DAKO K4001- STAG2) and Bajoran Purple chromogen kit (Biocare Medical BJP811). All slides were counterstained with hematoxylin (Vector H-3401). Stained slides were interpreted by a dedicated dermatopathologist.

Sequencing

Genomic DNA extracted from pre-treatment and post-relapse FFPE tissues of a patient who relapsed from vemurafenib treatment were subjected for whole exome sequencing analysis using Agilent SureSelect Human All Exon 51M kit at BGI (Beijing, China). Reads were mapped to hg19 using bwa[31]. PCR duplicates and non-uniquely mapped reads were discarded using samtools[32]. Varscan2[33] was further used to call somatic mutations and results were annotated by ANNOVAR[34]. Mutations mapped to segmental duplications or annotated in 1000 Genome Project and dbsnp138 were filtered afterwards. Only non-synonymous, stop-gain, stop-loss mutations were selected for later analysis. High confident mutations were further picked based on the total coverage, coverage for reference allele, coverage for altered allele and functional prediction from Polyphen2[35]. For high throughput Sanger sequencing, all coding exons and intron-exon junctions in the *STAG2* and *STAG3* genes were amplified by PCR, followed by DNA sequencing and SNP discovery data analysis at Polymorphic DNA Technologies (Alameda, CA). To confirm *STAG2* mutations found in patient samples and cell lines, PCRs were performed for Exon 7 and Exon 29 with the following pairs of primers: 7F, 5'-GATAGTGGAGATTATCCACTTAC-3', 7R, 5'-CTGCCAGGGTGCTTGTATGTCG-3'; 29F, 5'-ATGCCTATGCTCGCACAACT-3', 29R, 5'-ATACTGAGTCCATTTCCCTATGC-3'. NRAS Gly12Asp mutation in 501MEL cells[39]

were confirmed by PCR amplification of Exon 2 with primers: 2F, GAACCAAATGGAAGGTCACA and 2R, TGGGTAAAGATGATCCGACA followed by Sanger sequencing.

Materials

Information on the antibodies used in this study are listed in supplementary table 3. Validations of all antibodies are provided on the manufacturer's websites. Vemurafenib, dabrafenib and trametinib were purchased from Selleck Chemicals. Doxycycline, crystal violet and iodonitrotetrazolium chloride were purchased from Sigma. pLEX-HA-*DUSP6*-MYC was provided by Dr. Igor Astsaturov and pLJM1-*STAG2* by Dr. Todd Waldman through Addgene. pLX304-*DUSP4*-V5 was purchased from the DNASU Plasmid Repository. FLAG tag was added into the N-terminus of *DUSP4* to generate pLX304-FLAG-*DUSP4*-V5 using PCR-based methods. pBabe-FLAG-*STAG2* was generated by PCR-based subcloning from pLJM1-*STAG2*. pBabe-MYC-*BRAF* was generated by PCR-based subcloning from pLHCX-FLAG-*BRAF*[36]. pBabe-FLAG-*STAG3* was generated by PCR-based sub-cloning using *STAG3* cDNA purchased from GE Dharmacon as a template. Various *STAG2*, *STAG3* and *BRAF* mutants were generated using PCR mutagenesis and verified by sequencing. pLKO constructs containing shRNAs against human *STAG2* (shSTAG2#23:TRCN0000152523) and *STAG3* (shSTAG3#96: TRCN0000137596; shSTAG3#71: TRCN0000138271; shSTAG3#69: TRCN0000138869) were purchased from Sigma. pTRIPZ inducible lentiviral human *STAG2* shRNA (shSTAG2#60 CloneID:V2THS_12573) and *STAG3* shRNA (shSTAG3#55 CloneID:V3THS 301555) were purchased from GE Dharmacon.

Cell culture

All melanoma cell lines used in this study contain BRAF Val600Glu mutations, except otherwise indicated. A375 and SKMEL28 were purchased from ATCC. LOX-IVMI was obtained from NCI-DCTD repository. WM902, WM902-BR, WM983, WM983-BR, MEL1617 were obtained from Dr. Meenhard Herlyn (Wistar). Immortalized *Braf*-null MEFs were a gift from Dr. Catrin Pritchard[37]. 501MEL and SKMEL103 harboring *NRAS* mutations were gifts from Dr. Lynda Chin and Dr. Jonathon Zippin, respectively. These cell lines have not been authenticated by the authors. WM902, WM983, M14, MEL1617, SKMEL28, A375, LOX-IVMI, 501MEL and SKMEL103 cells were cultured in RPMI containing 10% fetal bovine serum (FBS) and penicillin/streptomycin/glutamine (PSG). HEK293 and mouse embryonic fibroblast (MEF) cells were maintained in DMEM containing 10% FBS and PSG. WM902-BR, WM983-BR, M14-BR, A375-BR and Mel1617-BR cells were maintained in complete media supplemented with vemurafenib or dabrafenib. A375-BMR and MEL1617-BMR cells were maintained in completed media supplemented with Dabrafenib and Trametinib. For the cell viability analysis, cells were seeded in a 96-well plates and drug treatment was started the following day. After 72 h incubation, MTS assay was performed according to manufacturer's instructions (Promega). All cell lines were tested negatively for mycoplasma with the MycoSensor PCR Assay Kit (Agilent Technologies). Transfection, retroviral and lentiviral infection were performed as previously described[25]. When indicated, stable populations were obtained and maintained by

selection with puromycin (Sigma). Clonogenic growth[25] and anchorage-independent growth soft agar assays[38] were performed as previously described.

Cell cycle and apoptosis analyses

For cell cycle analysis, cells were fixed dropwise with 70% ice cold ethanol for 30 min on ice and suspended in PBS containing 10 μg/ml of propidium iodide (PI) and 10 μg/ml of RNase A. PI-stained samples were analyzed for cell cycle progression by flow cytometry using a FACScalibur (Becton and Dickinson) apparatus, followed by data analysis using the FlowJo software (TreeStar). For apoptosis analysis, apoptotic cells were detected using BD FITC Annexin V Apoptosis Detection Kit followed by flow cytometry analysis.

Western blotting and immunoprecipitation

Western blotting and immunoprecipitation were performed as previously described[38]. RAS activity assay was performed using active RAS pull-down and detection kit according to manufacturer's instructions (Thermo Scientific). Briefly, 500 μg of cell lysates were incubated with GST-RAF1-RBD and glutathione resin at 4°C for 1 h. After washing, the active RAS was eluted by 2X reducing sample buffer and subjected for SDS-PAGE and immunoblotting.

Animal studies

All studies and procedures involving animal subjects were performed following Massachusetts General Hospital Institutional Animal Care and Use Committee (IACUC) guidelines. For xenograft models, 6-weeks-old female athymic mice ($NCr^{nu/nu}$) were purchased from Taconic farms. Animals were allowed a 1-week adaptation period after arrival. A375 cells (1×10^6 in 0.2 ml of basal culture medium) were injected subcutaneously in the right lateral flank. To induce silencing of STAG2 *in vivo*, 2 mg/mL doxycycline and 5% sucrose was added to the drinking water 13 days post inoculation. Doxycycline-containing water was changed every three days. Vemurafenib diet (1.42 g/kg to achieve a 25 mg/kg daily dose) and control diet were prepared at Harlan Laboratories (Madison, WI). Animals were randomly assigned to 4 groups that were administered vehicle (5% sucrose in water), doxycycline, vehicle and vemurafenib, or both doxycycline and vemurafenib, by the Research Randomizer at http://www.randomizer.org. The investigators were not blinded to group allocation or outcome assessment. No statistical method was used to predetermine sample size. Treatment began when the tumor volume reached between 80 to 120 mm^3. No animals were excluded in these experiments. Tumor dimensions were measured with calipers and volumes calculated using the following formula: $(D \times d^2)/2$, in which D represents the large diameter of the tumor, and d represents the small diameter of the tumor. Animals were sacrificed at the end of experiments or when tumor size reached 1.5 cm at any directions.

Mouse tissue sections were prepared for immunohistochemistry as previously described[25]. Briefly, harvested mouse tissues were fixed in 10% neutral buffered formalin and embedded in paraffin. Slides were deparaffinized using HistoChoice clearing reagent (Amresco) and rehydrated with water. Antigen retrieval for formalin fixed tissue sections was performed by heating slides in a pressure cooker for 10 min in citrate antigen retrieval solution. After wash

with PBS, endogenous peroxidase activity was quenched with 3% hydrogen peroxide in PBS for 10 min at room temperature. For pERK, STAG2 and STAG3 staining, slides were blocked with 5% goat serum in PBS for 30 min and incubated with the primary antibodies for STAG2 (1:100, Santa Cruz, SC-81852), STAG3 (1:200, Abcam Ab185109), pERK (1:400, Cell Signaling) at 4°C overnight, followed by incubation with biotinylated anti-rabbit IgG for pERK and STAG3, and anti-mouse IgG for STAG2 for 30 min (Vector Laboratories). All slides were then incubated with avidin-biotin peroxidase (ABC) complex for 30 min and the signals visualized using DAB Substrate Kit (Vector Laboratories). The tissue sections were counter-stained with Gill's hematoxylin QS and mounted with VectaMount after dehydration.

Reverse-Transcription and Real-Time qPCR

RNA samples were isolated using the RNeasy Mini kit (Qiagen) and reverse transcribed (~2 µg) using the RevertAid Reverse Transcription Kit (Thermo fisher scientific). qPCRs were performed using the SYBR Green I Master (Roche) on the Light Cycler 480 Real Time PCR instrument (Roche). Each sample was tested in triplicates, and results were normalized to the expression of the housekeeping *GAPDH* gene. Specific primer sequences used in this study were as follows:

DUSP4 forward, 5'-GGCTACATCCTAGGTTCGGT-3'

DUSP4 reverse, 5'-CAGGATCTGCTCCAGGCT-3';

DUSP6 forward, 5'-CTGCATTGCGAGACCAATCTA-3'

DUSP6 reverse, 5'-CATCCGAGTCTGTTGCACTATT-3';

GAPDH forward, 5'-ATCACTGCCACCCAGAAGAC-3';

GAPDH reverse, 5'-CAGTGAGCTTCCCGTTCAG-3'.

Chromatin immunoprecipitation

ChIP experiments were performed using the iDeal ChIP-seq Kit for Transcription Factors (Diagenode) according to the manufacturer's instructions. Briefly, cells were grown to 80–90% confluency and then fixed with 1% formaldehyde solution (Sigma). Eight million cells were used per IP. Chromatin was sonicated into 200 - 800 bp fragments, and 1% of the chromatin was used to purify the input DNA fragments. Chromatin was immunoprecipitated with CTCF antibody or nonspecific rabbit IgG. qRT–PCR using SYBR Green was performed to detect enriched DNA. Primers used for qPCR were as follows:

CTCF R1 forward, 5'-CTGAAGACTGTCCGAAATTATGC-3';

CTCF R1 reverse, 5'-CTGATTTCTCCCTACTGGTCAC-3';

CTCF R2 forward, 5'-CTCCAACAGGTTTGCTCTTCT-3';

CTCF R2 reverse, 5'-CCCGAGACGTTTCAGTCATT-3';

H19 forward, 5'-CTGGTCTGTGCTGGCCACGG-3';

H19 reverse, 5'-GCACCTTGGCTGGGGCTCTG-3'.

Supplementary Material

Refer to Web version on PubMed Central for supplementary material.

Acknowledgements

References

1. Ribas A, Flaherty KT. BRAF targeted therapy changes the treatment paradigm in melanoma. Nat Rev Clin Oncol. 2011; 8:426–433. [PubMed: 21606968]

2. Holderfield M, Deuker MM, McCormick F, McMahon M. Targeting RAF kinases for cancer therapy: BRAF-mutated melanoma and beyond. Nat Rev Cancer. 2014; 14:455–467. [PubMed: 24957944]

3. Moriceau G, et al. Tunable-combinatorial mechanisms of acquired resistance limit the efficacy of BRAF/MEK cotargeting but result in melanoma drug addiction. Cancer Cell. 2015; 27:240–256. [PubMed: 25600339]

4. Van Allen EM, et al. The genetic landscape of clinical resistance to RAF inhibition in metastatic melanoma. Cancer Discovery. 2014; 4:94–109. [PubMed: 24265153]

5. Shi H, et al. Acquired Resistance and Clonal Evolution in Melanoma during BRAF Inhibitor Therapy. Cancer Discovery. 2014; 4:80–93. [PubMed: 24265155]

6. Lito P, Rosen N, Solit DB. Tumor adaptation and resistance to RAF inhibitors. Nat Med. 2013; 19:1401–1409. [PubMed: 24202393]

7. Kwong LN, et al. Co-clinical assessment identifies patterns of BRAF inhibitor resistance in melanoma. J Clin Invest. 2015; 125:1459–1470. [PubMed: 25705882]

8. Wagle N, et al. MAP kinase pathway alterations in BRAF-mutant melanoma patients with acquired resistance to combined RAF/MEK inhibition. Cancer Discovery. 2014; 4:61–68. [PubMed: 24265154]

9. Long GV, et al. Increased MAPK reactivation in early resistance to dabrafenib/trametinib combination therapy of BRAF-mutant metastatic melanoma. Nature Communications. 2014; 5:5694.

10. Solomon DA, Kim J-S, Waldman T. Cohesin gene mutations in tumorigenesis: from discovery to clinical significance. BMB Reports. 2014; 47:299–310. [PubMed: 24856830]

11. Losada A. Cohesin in cancer: chromosome segregation and beyond. Nat Rev Cancer. 2014; 14:389–393. [PubMed: 24854081]

12. Kandoth C, et al. Mutational landscape and significance across 12 major cancer types. Nature. 2014; 502:333–339. [PubMed: 24132290]

13. Solomon DA, et al. Mutational Inactivation of STAG2 Causes Aneuploidy in Human Cancer. Science. 2011; 333:1039–1043. [PubMed: 21852505]

14. Balbás-Martínez C, et al. Recurrent inactivation of STAG2 in bladder cancer is not associated with aneuploidy. Nat Genet. 2013; 45:1464–1469. [PubMed: 24121791]

15. Guo G, et al. Whole-genome and whole-exome sequencing of bladder cancer identifies frequent alterations in genes involved in sister chromatid cohesion and segregation. Nat Genet. 2013; 45:1459–1463. [PubMed: 24121792]

16. Weinstein JN, et al. Comprehensive molecular characterization of urothelial bladder carcinoma. Nature. 2014; 507:315–322. [PubMed: 24476821]

17. Solomon DA, et al. Frequent truncating mutations of STAG2 in bladder cancer. Nat Genet. 2013; 45:1428–1430. [PubMed: 24121789]

18. Crompton BD, et al. The Genomic Landscape of Pediatric Ewing Sarcoma. Cancer Discovery. 2014; 4:1326–1341. [PubMed: 25186949]

19. Tirode F, et al. Genomic Landscape of Ewing Sarcoma Defines an Aggressive Subtype with Co-Association of STAG2 and TP53 Mutations. Cancer Discovery. 2014; 4:1342–1353. [PubMed: 25223734]

20. Thol F, et al. Mutations in the cohesin complex in acute myeloid leukemia: clinical and prognostic implications. Blood. 2014; 123:914–920. [PubMed: 24335498]

21. Thota S, et al. Genetic alterations of the cohesin complex genes in myeloid malignancies. Blood. 2014; 124:1790–1798. [PubMed: 25006131]

22. Yoshida K, et al. The landscape of somatic mutations in Down syndrome–related myeloid disorders. Nat Genet. 2013; 45:1293–1299. [PubMed: 24056718]

23. The Cancer Genome Atlas Research Network. Genomic and Epigenomic Landscapes of Adult De Novo Acute Myeloid Leukemia. New England Journal of Medicine. 2013; 368:2059–2074. [PubMed: 23634996]

24. Hodis E, et al. A Landscape of Driver Mutations in Melanoma. CELL. 2012; 150:251–263. [PubMed: 22817889]

25. Yuan P, et al. Phenformin enhances the therapeutic benefit of BRAFV600E inhibition in melanoma. Proc Natl Acad Sci USA. 2013; 110:18226–18231. [PubMed: 24145418]

26. Villanueva J, et al. Acquired Resistance to BRAF Inhibitors Mediated by a RAF Kinase Switch in Melanoma Can Be Overcome by Cotargeting MEK and IGF-1R/PI3K. Cancer Cell. 2010; 18:683–695. [PubMed: 21156289]

27. Ong C-T, Corces VG. CTCF: an architectural protein bridging genome topology and function. Nature Reviews Genetics. 2014; 15:234–246.

28. Xiao T, Wallace J, Felsenfeld G. Specific Sites in the C Terminus of CTCF Interact with the SA2 Subunit of the Cohesin Complex and Are Required for Cohesin-Dependent Insulation Activity. Mol Cell Biol. 2011; 31:2174–2183. [PubMed: 21444719]

29. Ziebarth JD, Bhattacharya A, Cui Y. CTCFBSDB 2.0: a database for CTCF- binding sites and genome organization. Nucleic Acids Research. 2012; 41:D188–D194. [PubMed: 23193294]

30. Katainen R, et al. CTCF/cohesin-binding sites are frequently mutated in cancer. Nat Genet. 2015; 47:818–821. [PubMed: 26053496]

31. Li H, Durbin R. Fast and accurate short read alignment with Burrows-Wheeler transform. Bioinformatics. 2009; 25:1754–1760. [PubMed: 19451168]

32. Li H, et al. The Sequence Alignment/Map format and SAMtools. Bioinformatics. 2009; 25:2078–2079. [PubMed: 19505943]

33. Koboldt DC, et al. VarScan 2: somatic mutation and copy number alteration discovery in cancer by exome sequencing. Genome Research. 2012; 22:568–576. [PubMed: 22300766]

34. Wang K, Li M, Hakonarson H. ANNOVAR: functional annotation of genetic variants from high-throughput sequencing data. Nucleic Acids Research. 2010; 38:e164–e164. [PubMed: 20601685]

35. Adzhubei IA, et al. A method and server for predicting damaging missense mutations. Nat Methods. 2010; 7:248–249. [PubMed: 20354512]

36. Shen C-H, et al. Phosphorylation of BRAF by AMPK Impairs BRAF-KSR1 Association and Cell Proliferation. Mol. Cell. 2013; 52:161–172. [PubMed: 24095280]

37. Kamata T, et al. A critical function for B-Raf at multiple stages of myelopoiesis. Blood. 2005; 106:833–840. [PubMed: 15784729]

38. Zheng B, et al. Oncogenic B-RAF negatively regulates the tumor suppressor LKB1 to promote melanoma cell proliferation. Mol. Cell. 2009; 33:237–247. [PubMed: 19187764]

39. Lin WM, et al. Modeling genomic diversity and tumor dependency in malignant melanoma. Cancer Research. 2008; 68:664–673. [PubMed: 18245465]
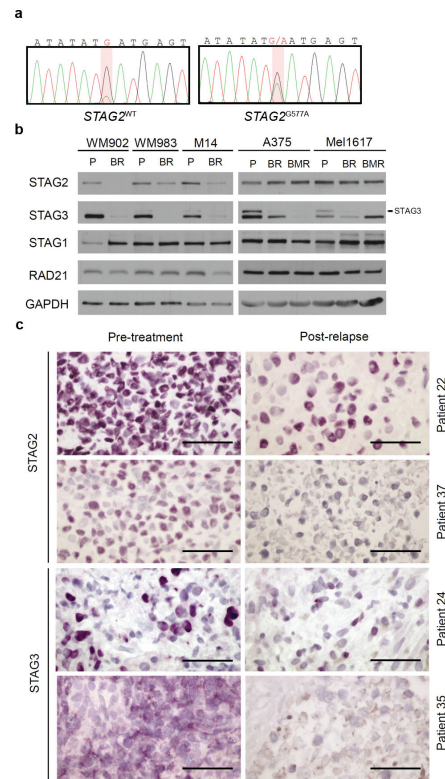
Figure 1. Decreased expression of STAG2 and STAG3 in BRAFi-resistant melanoma primary patient tumors and cell lines

(**a**) Sanger sequencing analysis of the *STAG2* locus in pre-treatment (left) and post-relapse (right) biopsies from a patient with recurrent disease following vemurafenib treatment. (**b**) Expression of cohesion complex components, STAG1, STAG2, STAG3 and RAD21 in a panel of melanoma BRAFi-resistant cell lines and their parental BRAFi-sensitive counterparts was measured by western blotting. GAPDH was used a loading control. P: parental; BR: BRAFi resistant. BMR: BRAFi and MEKi double resistant. (**c**) Immunohistochemical analyses of STAG2 and STAG3 in pairs of pre-treatment (left) and post-relapse (right) tumor samples from patients treated with BRAFi monotherapy or BRAFi and MEKi combination therapy. Two representative patients are shown for STAG2 and for STAG3. Scale bar: 50 microns.
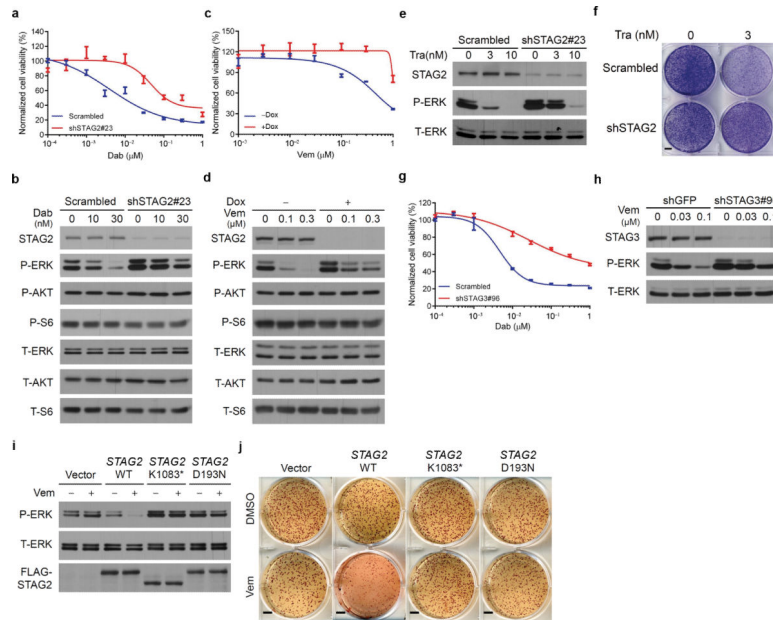
Figure 2. Knockdown of STAG2 or STAG3 decreases BRAFi sensitivity in BRAF mutant melanoma cells

(**a**) Viability of A375 cells after treatment with varying concentrations of dabrafenib for 3 d. Experiment was performed 3 times. Data are mean ± s.e.m. (**b**) A375 cells were treated with dabrafenib for 2 h. Cell lysates were used for western blotting with indicated antibodies. Experiment was performed 3 times. (**c**) Viability of SKMEL28 cells after treatment with varying concentrations of vemurafenib for 3 d. Experiment was performed 3 times. Data are mean ± s.e.m. (**d**) SKMEL28 cells were treated with vemurafenib for 2 h. Cell lysates were used for western blotting with indicated antibodies. Experiment was performed 3 times. (**e**) SKMEL30 cells were treated with trametinib for 2 h. Cell lysates were used for western blotting with indicated antibodies. Experiment was performed 3 times. (**f**) SKMEL30 cells were treated with trametinib as indicated in clonogenic growth assays. Experiment was performed 3 times. Scale bar: 5 mm. (**g**) Viability of A375 cells after treatment with varying concentrations of dabrafenib for 3 d. Experiment was performed 3 times. Data are mean ± s.e.m. (**h**) A375 cells were treated with vemurafenib for 2 h. Cell lysates were used for western blotting with indicated antibodies. Experiment was performed 3 times. (**i**) WM902-BR cells stably expressing control vector, FLAG-tagged wild-type STAG2 (WT), Lys1083* (K*) or Asp193Asn (DN) mutants were treated with 3 μM vemurafenib for 2 h. Cell lysates were used for western blotting with indicated antibodies. Experiment was performed 3 times. (**j**) WM902-BR cells were used in soft agar assays in the presence or absence of 3 μM vemurafenib. Experiment was performed 3 times. Scale bar: 5 mm.
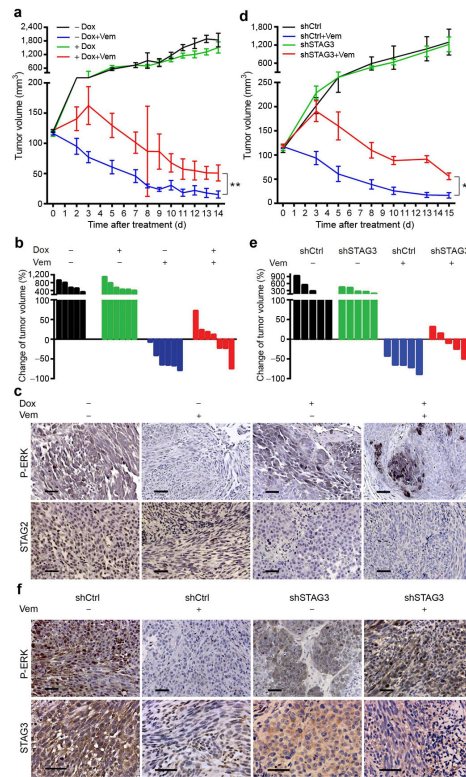
Figure 3. Knockdown of STAG2 or STAG3 impairs the effects of vemurafenib on inhibiting melanoma xenograft tumor growth *in vivo*

(**a**) Nude mice bearing xenograft tumors of A375 cells stably expressing pTRIPZ-shSTAG2#60 were treated with vehicle, doxycyline (Dox), vemurafenib (Vem), or both doxycyline and vemurafenib. Unpaired two-tailed Student's *t*-test was performed to compare between two groups of mice that were treated with vemurafenib (mean ± s.e.m. *P < 0.05*). The data variance is similar between groups. $n = 5$–7. (**b**) Waterfall plots showing the percent change in tumor volume at day 7 for the individual tumors in each treatment group of the STAG2 knockdown experiment. (**c**) Representative images of mouse tumor samples from the STAG2 knockdown experiment subjected for various immunohistochemical analyses as indicated. Scale bar: 50 μm. (**d**) Nude mice bearing xenograft tumors of A375 cells stably expressing pLKO-shSTAG3#69 were treated with control or vemurafenib (Vem) diet. Unpaired two-tailed Student's *t*-test was performed to compare between two groups of mice that were treated with vemurafenib (mean ± s.e.m. *P < 0.05).* The data variance is similar between groups. $n = 5$–7. (**e**) Waterfall plots showing the percent change in tumor volume at day 8 for the individual tumors in each treatment group of the STAG3 knockdown experiment. (**f**) Representative images of mouse tumor samples from the STAG3 knockdown experiment subjected for various immunohistochemical analyses as indicated. Scale bar: 50 μm.
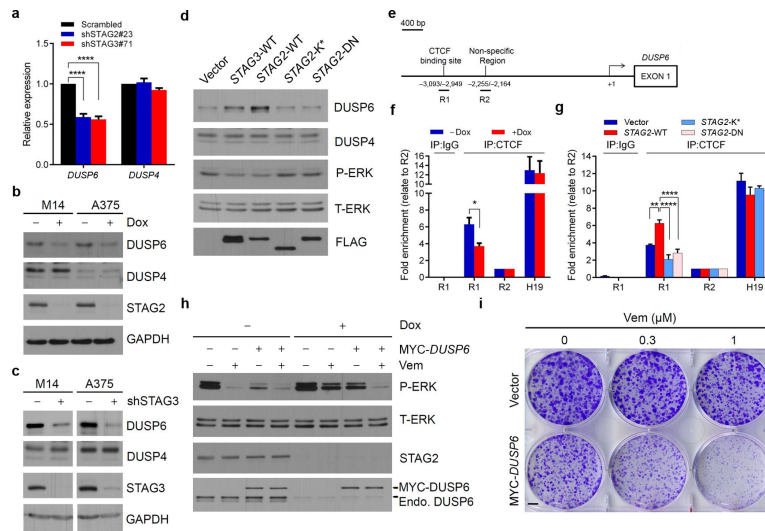
Figure 4. STAG2 regulates ERK activity through controlling expression of DUSP6
(**a**) Total RNA from A375 cells were isolated, reverse transcribed, and expression levels of *DUSP4* and *DUSP6* were analyzed by qPCR. mRNA levels were calculated relative to the scrambled control with housekeeping *GAPDH* gene as reference. $n = 3$ biological replicates. Data are mean ± s.e.m. The *P* values were determined using two-tailed Student's *t*-test, ***** P < 0.0001.* The data variance is similar between groups. (**b**) M14 or A375 cells expressing STAG2 inducible shRNA were cultured in the presence or absence of doxycycline for 5 d before lysates were used for western blotting with indicated antibodies. Experiment was performed 3 times. (**c**) Lysates from M14 or A375 cells expressing STAG3 shRNA#71 or scrambled control were used for western blotting with indicated antibodies. Experiment was performed 3 times. (**d**) Lysates from HEK293 cells transfected with indicated constructs were used for western blotting with indicated antibodies. K*, Lys1083*; DN, Asp193Asn. Experiment was performed 3 times. (**e**) Genomic structure of *DUSP6* gene showing the locations of amplified regions by ChIP-qPCR. R1: CTCF binding region, R2: non-specific region. (**f**) A375 cells expressing STAG2 inducible shRNA pTRIPZ-shSTAG2#60 were cultured in the presence or absence of doxycycline for 5 d before ChIP-qPCR assays were performed. Chromatins were immuoprecipitated using CTCF antibody or rabbit IgG. IP-ed chromatins were examined using qPCR with primers for R1 and R2 regions of *DUSP6* and *H19*. Results are expressed as fold enrichment relative to the non-specific region (R2). $n = 3$ biological replicates. Data are mean ± s.e.m. The *P* values were determined using two-tailed Student's *t*-test, ** P < 0.05.* The data variance is similar between groups. (**g**) Chromatins of LOX-IVMI cells stable expressing FLAG-tagged wild-type STAG2 (WT), Lys1083* (K*) or Asp193Asn (DN) mutants were immuoprecipitated using CTCF antibody or rabbit IgG. $n = 3$ biological replicates. Data are mean ± s.e.m. The *P* values were determined using two-tailed Student's *t*-test, *** P < 0.01; **** P < 0.0001.* The data variance is similar between groups. (**h**) A375 cells expressing STAG2 inducible shRNA pTRIPZ-shSTAG2#60 were infected with lentivirus expressing MYC-DUSP6 or control vector. Cells were cultured in the presence or absence of doxycycline for 5 d and treated with 0.3 µM vemurafenib for 2h before lysates were used for western blotting with indicated antibodies. Experiment was performed 3 times. (**i**) A375 cells expressing STAG2 inducible shRNA pTRIPZ-

shSTAG2#60 together MYC-tagged DUSP6 or control vector were treated with vemurafenib as indicated in clonogenic growth assays. Experiment was performed 3 times. Scale bar: 5 mm.